

# GW190521: A Binary Black Hole Merger in an AGN

Sophia Morton

*Department of Physics, Oregon State University, Corvallis, OR 97331 United States of America*

Advisors: Walter Del Pozzo and Stefano Rinaldi

*Dipartimento di Fisica “E. Fermi”, Università di Pisa, I-56127 Pisa, Italy and  
INFN, Sezione di Pisa, I-56127 Pisa, Italy*

(Dated: August 8, 2023)

We find evidence for a confident association between GW190521 and active galactic nucleus (AGN) flare ZTF19abanrhr using a model accounting for additional redshift of the gravitational wave source due to its location in the AGN. GW190521, detected by the LIGO-Virgo-KAGRA collaboration is the most massive binary black hole merger detected to date and the first detection of an intermediate-mass black hole.  $\sim 34$  days later the Zwicky Transient Facility detected flare ZTF19abanrhr in AGN J124942.3 + 344929 at the 78% spatial contour of GW190521’s sky localization. Given the association, GW190521’s location around the AGN’s supermassive black hole adds additional redshift contributions to the propagation of the gravitational wave between the source and detector frame. The multi-messenger nature of the event also allows for an estimation of Hubble constant which is consistent with the literature,  $103.1_{-25.0}^{+26.2}$  km s<sup>-1</sup> Mpc<sup>-1</sup> when analyzing solely GW190521 and  $79.4_{-9.3}^{+17.2}$  km s<sup>-1</sup> Mpc<sup>-1</sup> when including information from GW170817. In this work, GW190521 is found to have a negative relativistic redshift moving the primary mass of the merger from  $98.4_{-21.7}^{+33.6}$   $M_{\odot}$  to  $101.7_{-9.58}^{+21.5}$   $M_{\odot}$ , even further into the pair-instability supernova mass gap. This hypothesis is preferred over the lack of association with a log Bayes’ factor of 9.3, corresponding to an odds ratio of  $\sim 10000 : 1$  for equal prior odds and  $\sim 800 : 1$  for astrophysical prior odds. This indicates the first association of an electromagnetic signal with a binary black hole merger.

## I. INTRODUCTION

GW190521, a gravitational wave (GW) detected by the LIGO-Virgo-KAGRA collaboration (LVK) on May 21, 2019, is a reported merger between a  $\sim 98 M_{\odot}$  and a  $\sim 57 M_{\odot}$  black hole to produce a  $\sim 147 M_{\odot}$  intermediate-mass black hole. GW190521’s high mass fails to be explained by LVK power law + peak model for the mass distribution of black holes [1]. This model shows a mass gap at higher masses (65-120  $M_{\odot}$ ) due to the inability for astrophysical processes to form black holes in that mass range [2]. Many possible explanations have been proposed to reconcile these masses with the LVK mass distribution model, such as introducing larger orbital eccentricity [3, 4], modified gravity [5], or formation through dynamical capture [6].

In contrast, in AGN models the mass gap is not expected to be present due to the increased probability for hierarchical mergers and accretion [7]. Binary black holes (BBHs) in AGN are also predicted to have an electromagnetic counterpart caused by the interactions between the remnant black hole and AGN gas disk. Upon merging, the remnant moves with a kick velocity due to the significant loss of linear momentum from gravitational waves at the time of coalescence [2], heating the surrounding gas and leading to an increase in the AGN’s brightness.

However, the association between the EM counterpart and GW has been debated in prior works [8]. In previous analyses by Ashton *et al.* [8], an older data release [1] for GW190521 was used, favoring further luminosity distances and disfavoring distances corresponding to the EM

candidate,  $1.6(0.7)\sigma$  from the peak marginal luminosity distance as reported in Graham *et al.* [9] (see Figure 1).

The less significant luminosity distance overlap for the LVK posteriors samples released along with the discovery paper [1], lead to the inability to confidently associate GW190521 with the EM candidate previously, with odds ratios of 1 in 12 or less in favor of the association [8]. The updated LVK posterior samples set released in GWTC-2.1 [10] favors closer distances compared to Abbott *et al.* [1], as shown in Figure 1, with the EM counterpart distance lying at the 49<sup>th</sup> luminosity percentile for the distribution conditioned on the EM sky location and the 31<sup>st</sup> percentile for the distribution marginalized over the sky location. This significant change in the spatial overlap motivates the need for further analysis of the association given that a dominant factor in determining the odds of association is based on the luminosity distance. With updated posterior samples for the luminosity distance of GW190521 we find contrasting results with respect to Ashton *et al.* [8], providing a different answer to the question *is there an association between GW190521 and the EM counterpart candidate?*

In this work, the association with the EM counterpart is analyzed with respect to the LVK model. In our model under the assumption of the EM counterpart [9], the BBH is located in the disk of AGN J124942.3 + 344929, orbiting around a supermassive black hole (SMBH). This alters both the luminosity distance and source frame mass of the gravitational wave [11]. The LVK-reported source frame mass depends on the measured cosmological redshift since, akin to electromagnetic

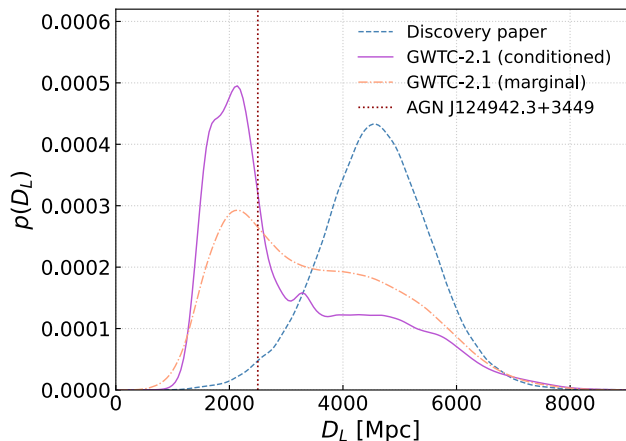


FIG. 1. Posteriors on luminosity distance for as in Abbott *et al.* [1] (blue), the LVK GWTC-2.1 posterior marginalized over sky location (orange), and conditioned on the sky location (purple) of AGN J124942.3 +3449 (vertical line in red). The older data release prefers further distances than the more recent LVK PE data.

waves, LVK is only sensitive to the detector frame mass, which has inherent cosmological redshift from the source frame. If the GW source has additional redshift due to external gravitational potentials or relativistic velocities the observed masses will be larger than when only cosmological redshift is present. In order for the masses to be out of the mass gap alternative formation channels [6] or a significant gravitational potential and velocity along the line of sight (LoS) are required. In contrast, negative redshift pushes masses even further into the mass gap.

In this report we first describe the effects of relativistic and gravitational redshift on the mass and luminosity distance of the GW signal in Sec. II A. The Bayesian statistical framework and models compared are then presented in Sec. II B. This is followed by a brief discussion of the computational and numerical methods used (Sec. III). Our results are presented for models with both a fixed and an unspecified Hubble constant in Sec. IV B, concluding with the odds ratios between the models in Sec. IV C.

## II. METHODS

### A. Theoretical model of a redshifted BBH

The relativistic and gravitational redshift only depend on the radial distance to the SMBH  $r$  in terms of Schwarzschild radii  $R_s$  and the angle between the BBH velocity and LoS. Geometric units ( $G=c=1$ ) are used throughout.

The velocity  $v$  in the source frame is dependent only on the BBH's distance from the SMBH, assuming a circular orbit,

$$v = \frac{1}{\sqrt{2\left(\frac{r}{R_s} - 1\right)}}. \quad (1)$$

The magnitude of the velocity can be transformed to the velocity along the line of sight (LoS),

$$v_{LoS} = v \cos(\theta), \quad (2)$$

via the angle between with velocity and the LoS  $\theta$ .

The relativistic redshift results from the motion along the LoS as well as the Lorentz factor  $\gamma$  due to the magnitude of the BBH's velocity,

$$z_{rel} = \gamma(1 + v_{LoS}) - 1. \quad (3)$$

The additional gravitational redshift from the SMBH potential is also only dependent on the BBH's orbital distance,

$$z_{grav} = \frac{1}{\sqrt{1 - \frac{r}{R_s}}} - 1. \quad (4)$$

The luminosity distance (dependent only on comoving distance  $r_d$  and cosmological redshift) and observer frame primary mass  $M_1^{\text{eff}}$  are thus transformed due to these additional sources of redshift as derived in Torres-Orjuela and Chen [11]:

$$D_{\text{app}} = (1 + z_{grav})(1 + z_{rel})^2 D_L \quad (5)$$

$$M_1^{\text{eff}} = (1 + z_c)(1 + z_{rel})(1 + z_{grav})M_1. \quad (6)$$

### B. Bayesian Statistical Framework

To determine the probability distribution for the primary mass and the amount of redshift given the gravitational wave data from LVK and the EM association, we worked in a Bayesian framework. Bayes' theorem provides a robust statistical framework for parameter estimation and model comparison.

The additional redshift depends only on the BBH's orbital distance  $r$  and orientation with respect to the LoS  $\theta$ . Ignoring the normalization constant for the purposes of parameter estimation, the probability of a given distance from the SMBH, source frame primary mass  $M_1$ , and angle is

$$p(r, M_1, \theta | d, z_c) \propto p(d | r, M_1, \theta, z_c) p(r, M_1, \theta). \quad (7)$$

The likelihood can be marginalized over the observed primary mass  $M_1^{\text{eff}}$  and apparent distance  $D_{\text{app}}$  as seen by the observer:

$$p(d|r, M_1, z_c) \propto \int \left[ p(d|D_{\text{app}}, M_1^{\text{eff}}, r, M_1, z_c) \times \right. \\ \left. \times p(D_{\text{app}}, M_1^{\text{eff}}|r, M_1, z_c) \right] dD_{\text{app}} dM_1^{\text{eff}}. \quad (8)$$

Given the association the probability distribution for  $M_1^{\text{eff}}$  and  $D_{\text{app}}$  are conditioned on the sky location of the EM counterpart using FIGARO. Here the probability of the data given the apparent distance and primary mass is given by the most up-to-date LVK data (GWTC-2.1), obtained via GWOSC [12], as well as a prior distribution for the apparent distance and primary mass:

$$p(d|D_{\text{app}}, M_1^{\text{eff}}) = \frac{p(D_{\text{app}}, M_1^{\text{eff}}|d)}{p(D_{\text{app}}, M_1^{\text{eff}})}. \quad (9)$$

The apparent distance and effective primary mass inherently depend on the relativistic and gravitational redshifts, which in turn depend on the effective angle and the BBH's velocity. The redshift values must be marginalized over to determine the probability distribution for the apparent distance and effective primary mass,

$$p(D_{\text{app}}, M_1^{\text{eff}}|r, M_1, z_c, \theta) = \\ = \int p(D_{\text{app}}, M_1^{\text{eff}}|r, M_1, z_c, \theta, D_L, z_{\text{rel}}, z_{\text{grav}}) \times \\ \times p(z_{\text{rel}}, z_{\text{grav}}, D_L|r, M_1, z_c, \theta) p(\theta|r, M_1, z_c) \times \\ \times d\theta dz_{\text{rel}} dz_{\text{grav}} dD_L. \quad (10)$$

The model chosen fixes the values of many parameters of interest, simplifying the probability distribution,

$$p(z_{\text{rel}}, z_{\text{grav}}, D_L|r, M_1, z_c, \theta) = \\ = \delta(z_{\text{rel}} - \gamma(1 + \frac{1}{\sqrt{2(\frac{r}{R_s} - 1)}}(\cos(\theta))) - 1) \\ \delta(z_{\text{grav}} - \sqrt{1 - \frac{R_s}{r}} - 1) \delta(f(z_c, H_0) - D_L). \quad (11)$$

Additionally, the apparent distance and effective mass given the source frame mass, luminosity distance, and redshifts (10) are also deterministic relationships and result in Dirac delta functions,

$$p(D_{\text{app}}, M_1^{\text{eff}}|r, M_1, z_c, \theta, D_L, z_{\text{rel}}, z_{\text{grav}}) = \\ = \delta(D_{\text{app}} - (1 + z_{\text{grav}})(1 + z_{\text{rel}})^2 D_L) \\ \delta(M_1^{\text{eff}} - (1 + z_c)(1 + z_{\text{rel}})(1 + z_{\text{grav}})M_1). \quad (12)$$

These relationships simplify the marginalization, resulting in a probability distribution that can be evaluated via Monte Carlo methods:

$$p(r, M_1|d, z_c) \propto \int \left[ \frac{p(D_{\text{app}}, M_1^{\text{eff}}|d)}{p(D_{\text{app}}, M_1^{\text{eff}})} \times \right. \\ \left. \times \delta(D_{\text{app}}) \delta(M_1^{\text{eff}}) \delta(z_{\text{rel}}) \delta(z_{\text{grav}}) \delta(D_L) p(r) p(M_1) \right] \times \\ \times dD_{\text{app}} dM_1^{\text{eff}} d\theta dz_{\text{rel}} dz_{\text{grav}}. \quad (13)$$

### 1. Priors

In this work, the prior for the primary mass  $p(M_1)$  is close to uniform, motivated by AGN mass distribution models [7].

The prior for the distance from the SMBH  $p(r)$  is based on the migration traps models in [13]. Migration trap locations at 24.5 and 331 Schwarzschild radii are approximated as Laplacian resonances centered at the migration trap location as shown in Figure 2, with a full width at half maximum of  $4.8 R_s$ . The model also depends linearly on the radial distance, to account for the overall axial symmetry of the system.

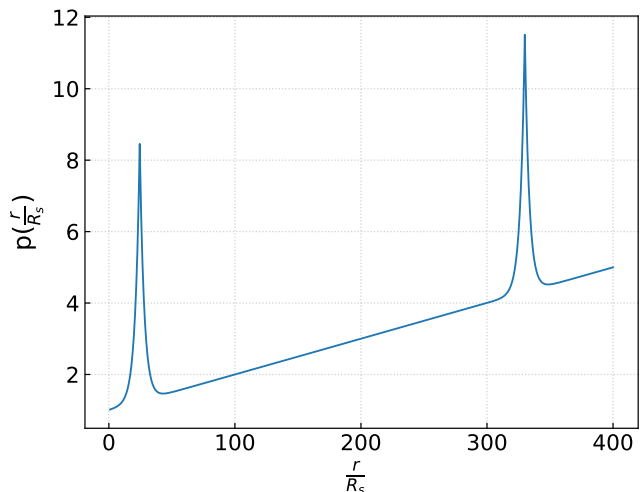


FIG. 2. The unnormalized prior on the distance of the BBH from the SMBH, given in terms of Schwarzschild radii  $R_s$ . The model is linear in distance with the addition of two Laplacians at migration trap locations

### 2. Model comparison

Bayes' theorem allows model comparison via a ratio of the evidence for the two models. The evidence can be thought of as the probability of the model as a whole, or the model probability marginalized over all of its parameters. The comparison of the evidence between two different hypothesis,  $H_1$  and  $H_2$ , is done via the Bayes' factor, or ratio of support for one model over another,

$$B_{12} = \frac{p(d|H_1)}{p(d|H_2)}, \quad (14)$$

where the ratio is between the evidence for each model. Given prior knowledge about the belief in one model versus the other, the odds ratio can tell us which model is favored,

$$O_2^1 = \frac{p(H_1|d)}{p(H_2|d)} = B_{12} \frac{p(H_1)}{p(H_2)}, \quad (15)$$

with higher odds favoring model 1 versus 2.

Bayes' factors and odds ratios are computed comparing each model against the agnostic, currently reported no association model shown in Table I.

### 3. Models

The models compared are:

- **No association:** The model in which the EM counterpart candidate and GW190521 are not associated. The prior on the primary mass is given by LVK's power law + peak model.
- **Association:** An association model between flare ZTF19abanrh and GW190521 in which the BBH is redshifted by its location in the AGN with the fixed Planck value of  $H_0$ . The sky location of the GW is conditioned on the EM location. The prior on the distance from the AGN's SMBH is shown in Figure 2 and the prior mass distribution is modelled after the mass distribution presented in Vaccaro and Mapelli [7].
- **Free  $H_0$ :** In this model we assume the association between the AGN flare and GW190521, but with the addition of freeing the Hubble constant. We used a flat in log prior for  $H_0$ .
- **GW170817 prior:** Similar to the Free  $H_0$  model, with the addition of the GW170817 Hubble constant posterior as a prior for  $H_0$

## III. COMPUTATIONAL METHODS

### A. Monte Carlo

Monte Carlo methods are based on principles of random sampling and are widely used in many fields of physics. The method relies on random sampling over a defined probability space. When the probability space is defined by a large set of parameters, Markov chain Monte Carlo (MCMC) is used due to its ability to numerically perform multidimensional integrals. Each chain starts at

a random point in the probability space and then walks towards regions of higher probability. The chain is allowed to also walk to regions of lower probability to explore the whole space. In this method, each point is correlated to the previous one because the walker can only move a limited distance from one point to the next.

### B. Nested sampling and RayNest

Nested Sampling [14] relies on Monte Carlo but is quicker and more efficient: moreover, it has the useful property of being able to reliably compute the evidence for a model. Draws are randomly distributed across a probability space initially and after each iteration, the datapoint with the lowest probability is removed and the region over which the sampler moves shrinks to exclude it. A new point is randomly drawn over this smaller space and this is iterated until the change in the evidence from one iteration to the next is sufficiently small. In this analysis, the RAYNEST<sup>1</sup> nested sampler was used. For computational purposes, the log probability space is used.

### C. FIGARO

FIGARO<sup>2</sup> (Fast Inference for GW Astronomy Research & Observations) estimates multivariate probability densities using nonparametric models [15]. FIGARO was used to reconstruct the probability density of the observed primary mass and luminosity distance from the LVK data. Thanks to the properties of the Gaussian Mixture Model this density was analytically conditioned on the EM sky location.

## IV. RESULTS

### A. Association model

Using RAYNEST to evaluate the probability distribution as defined in Sec. II B, the sampler recovers posteriors for the BBH's orbital position and source frame mass for the association model shown in Figure 3. The source frame mass depends on the redshift determined by the location of the BBH in its orbit around the SMBH as defined in equation 6. The relativistic and gravitational redshift are both higher when the BBH is closer to the SMBH.

The BBH's motion towards the Earth is favored, however, the posterior on the radial distance is consistent with the prior (Figure 2) other than slight deviations in

<sup>1</sup> Publicly available at <https://pypi.org/project/raynest/>

<sup>2</sup> Publicly available at <https://github.com/sterinaldi/FIGARO>.

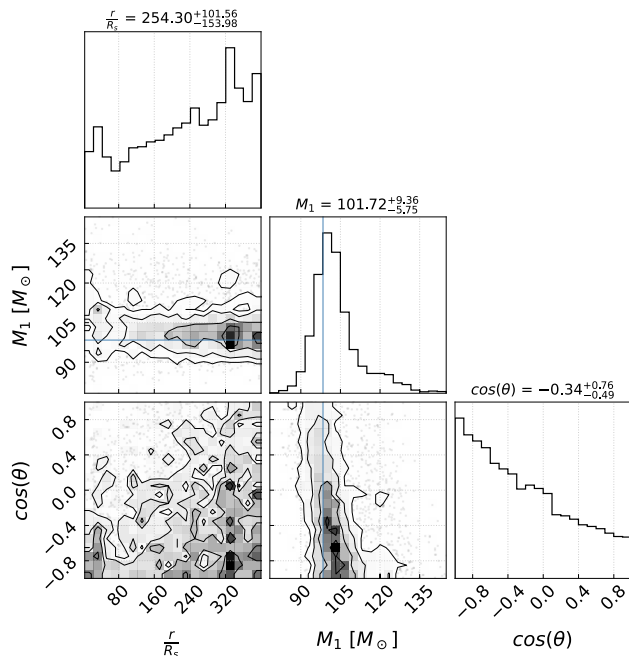


FIG. 3. Posterior samples for the model in which GW190521 is associated with the EM candidate and located in an AGN. The distance from the SMBH in terms of Schwarzschild radii and the effective angle relative to the LoS determine the amount of additional redshift. In turn, the redshift determines the source frame mass, with the LVK GWTC-2.1 reported mass shown as the vertical line in blue for comparison.

the innermost region ( $\lesssim 10R_s$ ), insensitive to its true value. The samples are taken over the cosine of the effective angle for simplicity, with a negative value defined as the BBH moving toward the Earth. This motion corresponds to a blueshift of the GW, leading to a detector frame mass that is smaller than the corresponding mass for a BBH at rest in the comoving frame. As seen in Figure 4 the source frame primary mass is shifted slightly towards a higher mass and is better constrained compared to LVK’s most recently reported value.

### B. Free $H_0$ and GW170817 prior models

GW events with EM counterparts can be used to determine the Hubble constant and ease the Hubble tension. By freeing the Hubble constant  $H_0$  within our model (Eqn. 11) we can recover a probability distribution for  $H_0$ . With a uniform prior (free  $H_0$  model), the Hubble constant is  $103.1^{+26.2}_{-25.0}$  km s $^{-1}$  Mpc $^{-1}$ .

Additionally, the independent multi-messenger event of neutron star merger GW170817 can be used as a prior for  $H_0$ . In the GW170817 prior model  $H_0$  is found to be  $79.4^{+17.2}_{-9.3}$  km s $^{-1}$  Mpc $^{-1}$ , consistent with Planck [16] and SH0ES [17], but closer to the SH0ES value of  $73.06^{+1}_{-1}$  km s $^{-1}$  Mpc $^{-1}$  (shown in Figure 5).

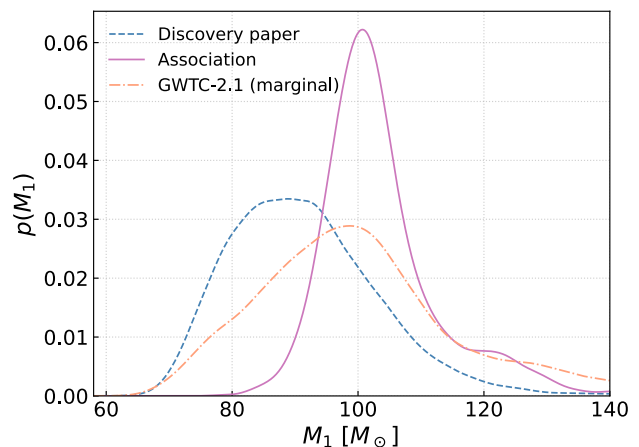


FIG. 4. Posterior distributions for the source frame primary mass for the model with the EM association and redshift contribution (pink) compared to two LVK reported models: O3 discovery paper posterior samples in blue and GWTC-2.1 in orange

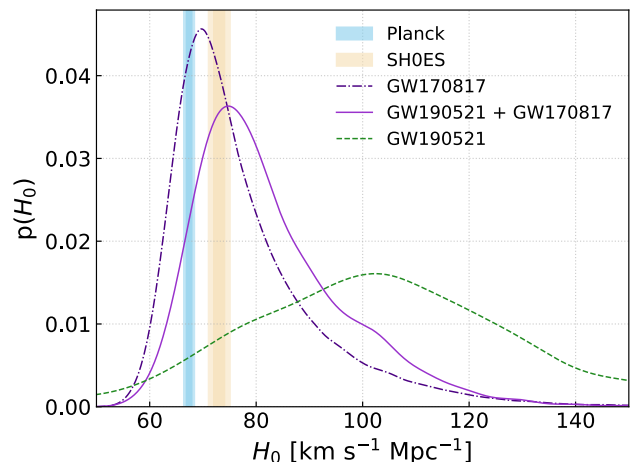


FIG. 5. Hubble constant posteriors for GW170817, GW190521, and GW190521 with GW170817 as a prior are compared to the reported values by Planck and SH0ES (shown with 1 and 2  $\sigma$  regions).

### C. Comparison to no EM Association Models

The log Bayes’ factors for the redshifted models compared to a no-association model with the prior on mass given as the LVK model of a power law + peak are shown in Table I. These factors were computed using the log evidence from RAYNEST. In Ashton *et al.* [8] the prior odds of the EM candidate not being associated with the GW event is given as the inverse of the number of events that could potentially be correlated. In order to confidently associate the EM counterpart candidate and GW events the log Bayes’ factor must be larger than this prior, given

as 1/13 [8]. The log odds ratio accounting for this prior is also given in Table I.

Model	$\log \mathcal{B}$	$\log \mathcal{O}$
Association	$9.3 \pm 0.1$	$6.7 \pm 0.1$
free $H_0$	$8.9 \pm 0.1$	$6.3 \pm 0.1$
GW170817 prior	$9.5 \pm 0.1$	$7.0 \pm 0.1$

TABLE I. Log Bayes' factors and odds ratios for the different models considered in this work compared to the no association model. We use 1/13 as astrophysical prior odds [8].

## V. CONCLUSIONS

The association of GW190521 with electromagnetic candidate counterpart ZTF19abnrhr inside an AGN is preferred to the LVK model with a log Bayes' factor of over 9. This model relies on the additional redshift of the BBH caused by its orbit around the AGN's SMBH, with odds ratios of 6.7, 6.3, and 7.0 for the association, free  $H_0$ , and GW170817 prior model assuming an astrophysical prior of 1/13 with respect to the no association model. The association model prefers a blueshifted BBH, increasing the source frame mass to  $101.7_{-5.75}^{+9.36} M_\odot$  compared to the no association LVK value of  $98.4_{-21.7}^{+33.6} M_\odot$ , moving the primary mass even further into the mass gap. The free  $H_0$  and GW170817 prior model values are also consistent with GWTC-2.1, with masses of  $100.3_{-5.88}^{+8.16} M_\odot$  and  $101.1_{-5.87}^{+9.44} M_\odot$  respectively. When freeing the Hubble constant in the model and using GW170817 as a prior, the posterior on  $H_0$ ,  $79.4_{-9.3}^{+17.2} \text{ km s}^{-1} \text{ Mpc}^{-1}$ , is consistent with both the SH0ES and Planck value. With respect to the existing literature – Mukherjee *et al.* [18], where the authors report a value of  $H_0 = 43.1_{-11.4}^{+24.6} \text{ km s}^{-1} \text{ Mpc}^{-1}$  obtained with the IMRPhenomPv3HM posterior samples from Abbott *et al.* [1] – we find a value of  $H_0 = 103.1_{-25.0}^{+26.2} \text{ km s}^{-1} \text{ Mpc}^{-1}$  with an agnostic prior distribution and GWTC-2.1 LVK data: this adds up as circumstantial evidence for the association. The EM association for GW190521 exhibits the behavior expected by a BBH in an AGN within the limitations of the EM data [9] and the association is strongly favored over the no association model.

## ACKNOWLEDGMENTS

We thank Alejandro Torres-Orjuela for providing the theoretical derivation that started this analysis and Maria Paola Vaccaro for providing the AGN formation channel black hole mass distribution. We are also grateful to both of them for the useful discussions.

This work was partially supported by the University of Florida's International Research Experience for Undergraduates program, funded by the NSF (Grant agreement NSF PHY-1950830).

This research has made use of data or software obtained from the Gravitational Wave Open Science Center (gwosc.org), a service of the LIGO Scientific Collaboration, the Virgo Collaboration, and KAGRA. This material is based upon work supported by NSF's LIGO Laboratory which is a major facility fully funded by the National Science Foundation, as well as the Science and Technology Facilities Council (STFC) of the United Kingdom, the Max-Planck-Society (MPS), and the State of Niedersachsen/Germany for support of the construction of Advanced LIGO and construction and operation of the GEO600 detector. Additional support for Advanced LIGO was provided by the Australian Research Council. Virgo is funded, through the European Gravitational Observatory (EGO), by the French Centre National de Recherche Scientifique (CNRS), the Italian Istituto Nazionale di Fisica Nucleare (INFN) and the Dutch Nikhef, with contributions by institutions from Belgium, Germany, Greece, Hungary, Ireland, Japan, Monaco, Poland, Portugal, Spain. KAGRA is supported by Ministry of Education, Culture, Sports, Science and Technology (MEXT), Japan Society for the Promotion of Science (JSPS) in Japan; National Research Foundation (NRF) and Ministry of Science and ICT (MSIT) in Korea; Academia Sinica (AS) and National Science and Technology Council (NSTC) in Taiwan.

## THANKS

I would like to personally thank Walter Del Pozzo and Stefano Rinaldi for their endless support and encouragement this summer and the countless lessons they have taught me.

## DATA AVAILABILITY

The code used to produce the results presented in this report is available at the following URL: <https://github.com/phiamorton/GW190521>.

GW190521 posteriors samples are obtained via GWOSC: <https://gwosc.org/eventapi/html/GWTC-2.1-confident/GW190521/v4/>.

- 
- [1] R. Abbott *et al.*, GW190521: A Binary Black Hole Merger with a Total Mass of  $150 M_{\odot}$ , *Phys. Rev. Lett.* **125**, 101102 (2020), [arXiv:2009.01075 \[gr-qc\]](#).
- [2] R. Abbott *et al.*, Properties and Astrophysical Implications of the  $150 M_{\odot}$  Binary Black Hole Merger GW190521, *ApJL* **900**, L13 (2020), [arXiv:2009.01190 \[astro-ph.HE\]](#).
- [3] V. Gayathri, J. Healy, J. Lange, B. O'Brien, M. Szczepanczyk, I. Bartos, M. Campanelli, S. Klimenko, C. Lousto, and R. O'Shaughnessy, Eccentricity Estimate for Black Hole Mergers with Numerical Relativity Simulations, [arXiv e-prints](#), [arXiv:2009.05461 \(2020\)](#), [arXiv:2009.05461 \[astro-ph.HE\]](#).
- [4] I. Romero-Shaw, P. D. Lasky, E. Thrane, and J. Calderón Bustillo, GW190521: Orbital Eccentricity and Signatures of Dynamical Formation in a Binary Black Hole Merger Signal, *ApJL* **903**, L5 (2020), [arXiv:2009.04771 \[astro-ph.HE\]](#).
- [5] Y.-F. Wang, S. M. Brown, L. Shao, and W. Zhao, Tests of gravitational-wave birefringence with the open gravitational-wave catalog, *Phys. Rev. D* **106**, 084005 (2022), [arXiv:2109.09718 \[astro-ph.HE\]](#).
- [6] R. Gamba, M. Breschi, G. Carullo, S. Albanesi, P. Retegno, S. Bernuzzi, and A. Nagar, GW190521 as a dynamical capture of two nonspinning black holes, *Nature Astronomy* **7**, 11 (2023), [arXiv:2106.05575 \[gr-qc\]](#).
- [7] M. P. Vaccaro and M. Mapelli, Mass distribution of binary black holes in AGN disks (in preparation).
- [8] G. Ashton, K. Ackley, I. M. Hernandez, and B. Piotrkowski, Current observations are insufficient to confidently associate the binary black hole merger GW190521 with AGN J124942.3 + 344929, *Classical and Quantum Gravity* **38**, 235004 (2021), [arXiv:2009.12346 \[astro-ph.HE\]](#).
- [9] M. J. Graham *et al.*, Candidate Electromagnetic Counterpart to the Binary Black Hole Merger Gravitational-Wave Event S190521g\*, *Phys. Rev. Lett.* **124**, 251102 (2020), [arXiv:2006.14122 \[astro-ph.HE\]](#).
- [10] R. Abbott *et al.*, GWTC-2.1: Deep Extended Catalog of Compact Binary Coalescences Observed by LIGO and Virgo During the First Half of the Third Observing Run, [arXiv e-prints](#), [arXiv:2108.01045 \(2021\)](#), [arXiv:2108.01045 \[gr-qc\]](#).
- [11] A. Torres-Orjuela and X. Chen, Moving gravitational wave sources at cosmological distances: Impact on the measurement of the Hubble constant, *Phys. Rev. D* **107**, 043027 (2023), [arXiv:2210.09737 \[astro-ph.CO\]](#).
- [12] The LIGO Scientific Collaboration, the Virgo Collaboration, the KAGRA Collaboration, R. Abbott, *et al.*, Open data from the third observing run of LIGO, Virgo, KAGRA and GEO, [arXiv e-prints](#), [arXiv:2302.03676 \(2023\)](#), [arXiv:2302.03676 \[gr-qc\]](#).
- [13] J. M. Bellovary, M.-M. Mac Low, B. McKernan, and K. E. S. Ford, Migration Traps in Disks around Supermassive Black Holes, *ApJL* **819**, L17 (2016), [arXiv:1511.00005 \[astro-ph.GA\]](#).
- [14] J. Skilling, Nested sampling for general Bayesian computation, *Bayesian Analysis* **1**, 833 (2006).
- [15] S. Rinaldi and W. Del Pozzo, Rapid localization of gravitational wave hosts with FIGARO, *MNRAS* **517**, L5 (2022), [arXiv:2205.07252 \[astro-ph.IM\]](#).
- [16] Planck Collaboration, N. Aghanim, *et al.*, Planck 2018 results. VI. Cosmological parameters (Corrigendum), *A&A* **652**, C4 (2021).
- [17] Riess *et al.*, A Comprehensive Measurement of the Local Value of the Hubble Constant with  $1 \text{ km s}^{-1} \text{ Mpc}^{-1}$  Uncertainty from the Hubble Space Telescope and the SH0ES Team, *ApJL* **934**, L7 (2022), [arXiv:2112.04510 \[astro-ph.CO\]](#).
- [18] S. Mukherjee, A. Ghosh, M. J. Graham, C. Karathanasis, M. M. Kasliwal, I. Magaña Hernandez, S. M. Nissanke, A. Silvestri, and B. D. Wandelt, First measurement of the Hubble parameter from bright binary black hole GW190521, [arXiv e-prints](#), [arXiv:2009.14199 \(2020\)](#), [arXiv:2009.14199 \[astro-ph.CO\]](#).